J. Plasma Physics (2008), *vol.* 74, *part* 4, *pp.* 531–554. © 2008 Cambridge University Press
doi:10.1017/S0022377808007101 Printed in the United Kingdom

Annular self-similar solutions in ideal magnetogasdynamics

R. M. LOCK[1] and A. J. MESTEL[2]

[1] AWE, Reading, Berkshire RG7 4PR, UK
(r.lock@ic.ac.uk and rober.lock@awe.co.uk)
[2] Department of Mathematics, Imperial College, London SW7 2AZ, UK

(Received 19 July 2007 and accepted 31 December 2007, first published online 26 February 2008)

Abstract. We consider the possibility of self-similar solutions describing the implosion of hollow cylindrical annuli driven by an azimuthal magnetic field, in essence a self-similar imploding liner z-pinch. We construct such solutions for gasdynamics, for ideal '$\beta = 0$' plasma and for ideal magnetogasdynamics (MGD). In the latter two cases some quantities are singular at the annular boundaries. Numerical solutions of the full ideal MGD initial value problem indicate that the self-similar solutions are not attractive for arbitrary initial conditions, possibly as a result of flux-freezing.

1. Introduction

In z-pinch plasma confinement experiments researchers are often interested in imploding hollow, cylindrical (annular) plasmas; of particular interest is the use of these implosions to generate powerful pulses of thermal X-ray radiation [1]. Theoretical work in this field makes heavy use of computational simulation, particularly using various forms of magnetohydrodynamic (MHD) code, in order understand the conversion of driver energy into radiation [2–4].

In this paper we explore the possibility of self-similar, imploding, finite annular z-pinch solutions to the equations of ideal MGD (magnetogasdynamics for a perfect gas at infinite magnetic Reynolds number). We do not consider axial variation or instability. Liberman and Velikovich [5] developed and studied the equations of cylindrical ideal self-similar MGD, which can be seen as a direct extension of the work of Von Guderley [6] and others who studied self-similar flows in gasdynamics. An excellent review of self-similar gasdynamics was produced by Meyer-ter-Vehn and Schalk [7]. The addition of magnetic fields and forces to the equations of gasdynamics, thereby giving MGD, requires the similarity ansatz to be extended [5]. The similarity equations studied here are essentially those of Liberman and Velikovich [5] but our notation is closer to that of Meyer-ter-Vehn and Schalk [7].

In Sec. 2 we introduce the ideal cylindrical MGD similarity equations and discuss some of their general features. Among these is the fact that the ideal MGD similarity equations may be cast as a three-dimensional autonomous system with two complete two-dimensional sub-systems, in which either the magnetic pressure or the fluid pressure vanishes.

In Secs 3 and 4 we discuss the possibility of imploding finite annular solutions to the equations represented by these sub-systems. In Sec. 5 we seek such annular

https://doi.org/10.1017/S0022377808007101 Published online by Cambridge University Press

solutions for the full three-dimensional system and develop constraints on the similarity parameters for such solutions to exist. We show that annular solutions are possible but that they must have singularities at the boundaries. Finally, in Sec. 6 we consider whether hollow annular solutions of the full MGD initial value problem are attracted to self-similar solutions under the imposition of appropriate boundary conditions.

2. The equations of self-similar cylindrical ideal MGD

Consider a cylindrically symmetric annulus of highly conducting ideal gas carrying a current in the axial ($\mathbf{e}_z$) direction; in other words a hollow z-pinch. Under these conditions the magnetic field vector will be purely azimuthal. The symmetry of this configuration leads to a purely radial flow. The continuity, energy, momentum and magnetic equations can then, respectively, be written [8]

$$\rho_t + u\rho_r = -\rho\frac{(ru)_r}{r}, \tag{2.1}$$

$$(c^2)_t + u(c^2)_r = -(\gamma-1)c^2\frac{(ru)_r}{r}, \tag{2.2}$$

$$\rho(u_t + uu_r) = -\frac{1}{\gamma}(\rho c^2)_r - \frac{(r^2h^2)_r}{2r^2}, \tag{2.3}$$

$$h_t = -(uh)_r. \tag{2.4}$$

Here r is the cylindrical radial coordinate, t is time, $\rho(r,t)$ is density, $u(r,t)$ is the radial fluid velocity, $c(r,t)$ is the fluid sound-speed, $h(r,t)$ is the azimuthal magnetic field and $\gamma = c_\mathrm{p}/c_\mathrm{v}$ is the ratio of specific heats of the fluid. When a numerical value is required, we use $\gamma = 5/3$, the value for a monatomic ideal gas. We work with sound-speed and density throughout but the fluid pressure may be determined as $p(r,t) = \rho c^2/\gamma$ (the first term on the right-hand side of (2.3) can be seen to be the usual pressure gradient force density). The fluid temperature $T(r,t)$ and specific internal energy $e(r,t)$ are both directly proportional to the sound-speed squared. The equations of gasdynamics for a cylindrically symmetric flow are recovered by setting $h \equiv 0$.

We seek self-similar solutions of (2.1)–(2.4) and thus introduce the similarity variable X

$$X := \frac{r}{|t|^{1/\nu}} \tag{2.5}$$

and the associated real parameter ν. We note that for $1/\nu > 0$ implosions correspond to t negative and increasing. We start with the similarity ansatz given by Meyer-ter-Vehn and Schalk for gasdynamics [7]:

$$u(r,t) = \frac{1}{\nu}\frac{r}{t}U(X), \quad c(r,t) = \frac{1}{\nu}\frac{r}{t}C(X), \quad \rho(r,t) = r^{2(\lambda+\nu)}G(X). \tag{2.6}$$

Here λ is a second real similarity parameter and $U(X)$, $C(X)$ and $G(X)$ are to be found subject to suitable boundary conditions. This similarity structure must be extended to incorporate the magnetic field, which is possible if

$$h(r,t) = \frac{r^{1+\lambda+\nu}}{|t|}H(X). \tag{2.7}$$

https://doi.org/10.1017/S0022377808007101 Published online by Cambridge University Press

Substituting the trial solution, (2.6) and (2.7), into the equations of motion leads to the following system of ordinary differential equations (ODEs)

$$(U-1)U' + \frac{2}{\gamma}CC' + \frac{1}{\gamma}C^2(\ln G)' + \nu^2\frac{H}{G}H' + \frac{2(1+\lambda+\nu)}{\gamma}C^2 + U(U-\nu) + (2+\lambda+\nu)\nu^2\frac{H^2}{G} = 0, \tag{2.8}$$

$$(U-1)C' + \frac{(\gamma-1)}{2}CU' + C(\gamma U-\nu) = 0, \tag{2.9}$$

$$(U-1)(\ln G)' + U' + 2(1+\lambda+\nu)U = 0, \tag{2.10}$$

$$(U-1)(\ln H)' + U' + (2+\lambda+\nu)U - \nu = 0. \tag{2.11}$$

Here a prime refers to differentiation with respect to $\xi := \ln X$ and not X itself. Introducing ξ enables the system to be written in autonomous form.

The dimensionality of the system (2.8)–(2.11) can be reduced from four to three by the introduction of the variable

$$W := \frac{\nu^2 H^2}{G}, \tag{2.12}$$

which physically is the self-similar analogue of the Alfvén wave speed squared. If for convenience we further define the new variable

$$V := C^2, \tag{2.13}$$

the system takes the form

$$\frac{dU}{d\xi} = \frac{2V(\gamma U+1+\lambda) - \gamma U(U-1)(U-\nu) + \gamma(2+\lambda)W}{\gamma((U-1)^2 - V - W)} \tag{2.14}$$

$$\frac{dV}{d\xi} = -\frac{V}{(U-1)}((\gamma-1)U' + 2(\gamma U-\nu)) \tag{2.15}$$

$$\frac{dW}{d\xi} = -\frac{W}{(U-1)}(U' + 2(U-\nu)). \tag{2.16}$$

Equations (2.14)–(2.16) were given by Liberman and Velikovich [5].

2.1. Free-surface boundary conditions

We are interested in solutions to (2.14)–(2.16) which describe a fluid annulus of finite thickness, so that we have two free boundaries. At a free-surface with radial trajectory $r = r_0(t)$ the solution must satisfy the kinematic boundary condition [9]

$$\frac{D}{Dt}(r - r_0(t))\bigg|_{r=r_0(t)} = 0, \tag{2.17}$$

where D/Dt is the usual convective derivative. For a self-similar solution, the surface will occur at some fixed value of $X = X_b$ (the boundary value), so that $r_0(t) = X_b|t|^{1/\nu}$. Equation (2.17) then requires that the velocity variable must satisfy $U(X_b) = 1$. For an annular solution, with fluid in $X_{\text{in}} < X < X_{\text{out}}$ we must have

$$U(X_{\text{in}}) = 1 = U(X_{\text{out}}). \tag{2.18}$$

https://doi.org/10.1017/S0022377808007101 Published online by Cambridge University Press

Table 1. Finite critical points of (2.14)–(2.16).

U_c	V_c	W_c
0	0	0
ν	0	0
$\frac{\nu}{\gamma}$	$\frac{\nu^2(\nu-\gamma)(1-\gamma)}{\gamma(2\nu+2+2\lambda)}$	0
ν	0	Anything if $(2+\lambda)=0$

2.2. Some Observations on the (U, V, W) system

A physical solution to the system (2.14)–(2.16) requires $V \geqslant 0$ and $W \geqslant 0$, because we wish for C and $\sqrt{W}$ to be real.

Clearly the plane $U \equiv 1$ plays an important role in these equations because for arbitrary ν and λ, (2.15) and (2.16) are singular there. The equations are also generally singular on the surface

$$(U-1)^2 - V - W = 0 \tag{2.19}$$

the roots of this equation, $U \pm \sqrt{V+W} = 1$, are referred to by Meyer-ter-Vehn and Schalk as the limiting characteristics [7]. The singular surface divides the space into regions which are in or out of causal contact with the origin $r = 0$ at time $t = 0$; a signal launched from a point in the fluid with characteristic speed $U \pm \sqrt{V+W}$ may or may not reach the origin at $t = 0$, the limiting characteristics mark the interface between these regions.

Trajectories in the (U, V^+, W^+) space cannot cross the singular surface (2.19), except possibly at *special points*, (U_s, V_s, W_s), for which the numerator and denominator of (2.14) vanish simultaneously. The point $(1, 0, 0)$ is always such a special point regardless of the values of ν and λ.

Table 1 gives a list of the finite critical points of the system. Some authors lump what we have called special points in with the critical points, but we have chosen to keep the two separate as the solution behaviour is quite different in the two cases.

The planes $W \equiv 0$ and $V \equiv 0$ form two closed two-dimensional sub-systems of the MGD similarity equations, (2.14)–(2.16). If $W \equiv 0$ the magnetic field vanishes and we simply recover the similarity equations for ideal cylindrical gasdynamics. The second case ($V \equiv 0$) corresponds to a '$\beta = 0$ plasma' (where $\beta := 2\mu_0 p/B^2$; gasdynamics corresponds to $\beta \to \infty$) in which the magnetically generated forces completely dominate the internal fluid stresses (∇p). We are chiefly interested in annular solutions of the full (U, V, W) system but it is instructive first to study the (U, W) and (U, V) sub-systems somewhat. Although gasdynamic solutions of the (U, V) system cannot generally be identified with z-pinch implosions we describe a solution which can, in a special sense, be interpreted in just this way.

3. An annular solution of the gasdynamic (U, V) system

The (U, V) gasdynamic system is

$$\frac{dU}{d\xi} = \frac{2V(\gamma U + 1 + \lambda) - \gamma U(U-1)(U-\nu)}{\gamma((U-1)^2 - V)}, \tag{3.1}$$

$$\frac{dV}{d\xi} = -\frac{V}{(U-1)}((\gamma-1)U' + 2(\gamma U - \nu)). \tag{3.2}$$

https://doi.org/10.1017/S0022377808007101 Published online by Cambridge University Press

Similarity solutions of gasdynamics have been studied extensively [7] and we limit our discussion to a solution of particular interest.

It is possible to find solutions of (3.1) and (3.2) with $U \equiv 1$ for all ξ in the domain of the solution. Clearly such a solution is a candidate for a hollow annular flow since it satisfies the kinematic condition at all points. Substituting $U \equiv 1$ (and $U' = 0$) in (3.1) and (3.2) we note we require that $\gamma + \lambda + 1 = 0$ and $\nu = \gamma$. For these values of the similarity parameters, any functions V and G such that

$$V' + V(\ln G)' = \gamma(\gamma - 1) \tag{3.3}$$

satisfy the governing equations (2.2) and (2.3). However, if we seek a non-isolated solution continuous in ν and λ so that $U'/(U-1)$ tends to a finite limit, then from (3.1) we obtain

$$\lim_{U \to 1} \frac{U'}{U-1} = -2 - \frac{\gamma - 1}{V} \tag{3.4}$$

and, thus, (3.2) reduces to

$$\frac{dV}{d\xi} = (\gamma - 1)^2 - 2V, \tag{3.5}$$

which may readily be integrated. Then, returning to (2.8) (with $H \equiv 0$) to find G, we have the complete solution

$$U(X) = 1, \tag{3.6}$$

$$V(X) = \frac{(\gamma - 1)^2}{2} - \frac{A}{X^2}, \tag{3.7}$$

$$G(X) = DX^2 \left[\frac{(\gamma - 1)^2}{2} X^2 - A \right]^{1/(\gamma - 1)}, \tag{3.8}$$

where A and D are constants of integration.

If $A > 0$ in (3.7) and (3.8) then $G(X)$ is only defined for $X \geqslant \sqrt{2A/(\gamma-1)^2}$ and vanishes on the equality. With $A > 0$ then, the solution describes a hollow annulus of fluid with its inner boundary at $X_{\text{in}} = \sqrt{2A/(\gamma-1)^2}$, X_{out} may be anything greater than X_{in}. $V(X)$ also vanishes at X_{in} as does the fluid pressure.

This solution is the cylindrical equivalent of the spherical solution developed by Kidder in the context of ICF implosions [7, 10].

The physical flow variables for this solution take the form

$$u(r,t) = \frac{1}{\gamma} \frac{r}{t}, \tag{3.9}$$

$$c(r,t)^2 = \frac{1}{\gamma^2} \frac{r^2}{t^2} \left[\frac{(\gamma - 1)^2}{2} - A \frac{|t|^{2/\gamma}}{r^2} \right], \tag{3.10}$$

$$\rho(r,t) = \frac{D}{|t|^{2/\gamma}} \left[\frac{(\gamma - 1)^2}{2} \frac{r^2}{|t|^{2/\gamma}} - A \right]^{1/(\gamma - 1)}, \tag{3.11}$$

$$p(r,t) = \frac{D}{\gamma^3} \frac{1}{t^2} \left[\frac{(\gamma - 1)^2}{2} \frac{r^2}{|t|^{2/\gamma}} - A \right]^{\gamma/(\gamma - 1)}. \tag{3.12}$$

Taking $A > 0$, with $t < 0$ and increasing, this solutions represents the implosion of a hollow annulus of gas, with $\rho(r_{\text{in}}, t) = 0$ for all t, with its ultimate collapse occurring

https://doi.org/10.1017/S0022377808007101 Published online by Cambridge University Press

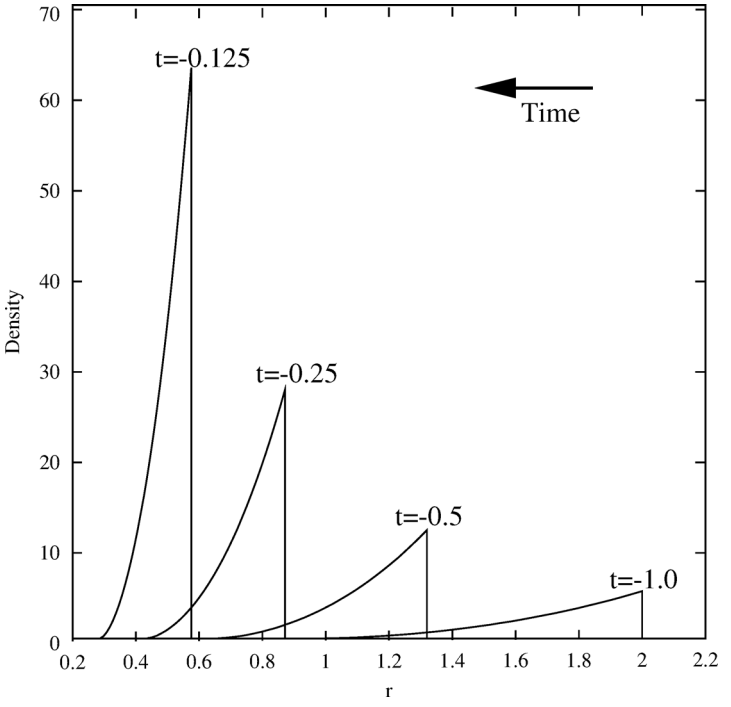


Figure 1. Density profiles for a self-similarly collapsing annulus of gas as a function of time, see (3.11). Time is negative and increasing. Collapse occurs at $t = 0$.

at $t = 0$. Figure 1 shows demonstrative density profiles throughout the history of the collapse. The flow is driven by an excess external pressure of magnitude

$$p_{\rm ext}(t) = \frac{D}{\gamma^3}\frac{1}{t^2}\left[\frac{(\gamma-1)^2}{2}(X_{\rm out}^2 - X_{\rm in}^2)\right]^{\gamma/(\gamma-1)}. \tag{3.13}$$

Essentially $p_{\rm ext}(t) \sim 1/t^2$. Although there is no magnetic field here, we can regard this external pressure to be magnetic in origin, generated by a current $I(t)$ carried in an infinitesimal skin layer at the outer boundary. This implies that $h \sim 1/t$ as $p_{\rm ext} = h^2/2$ and, since $h \sim I(t)/r_{\rm out}(t)$, we infer that the current becomes singular as

$$I(t) \sim |t|^{(1-\gamma)/\gamma} \quad (I \sim |t|^{-\frac{2}{5}} \text{ for } \gamma = \tfrac{5}{3}). \tag{3.14}$$

The solution discussed in this section, the cylindrical equivalent of Kidder's spherical solution [10], is only possible for a very particular choice of similarity constants, a choice which leads to the cancellation of various singularities in the similarity ODEs. In general, the equations are singular on $U = 1$, where this solution resides.

4. The (U, W) ($\beta = 0$) sub-system

The (U, W) sub-system can be written

$$\frac{dU}{d\xi} = \frac{(2+\lambda)W - U(U-1)(U-\nu)}{(U-1)^2 - W}, \tag{4.1}$$

https://doi.org/10.1017/S0022377808007101 Published online by Cambridge University Press

$$\frac{dW}{d\xi} = -W\left[\frac{W(2+\lambda+2\nu-2U)+U(U-\nu)(U-2)}{(U-1)((U-1)^2-W)}\right]. \tag{4.2}$$

The possibility of *special points* (see Sec. 2.1) in the (U, W) system is determined by the existence of real solutions to the cubic in U_s

$$0 = (U_s-1)[U_s^2-(2+\lambda+\nu)U_s+(2+\lambda)], \tag{4.3}$$

where the coordinates of the special point would be $(U_s, (U_s-1)^2)$. The trivial solution, $(1, 0)$ has already been noted in the full (U, V, W) system. An additional pair of special points exists if the descriminant of the remaining quadratic factor is positive. This is the case if $2+\lambda < 0$, and also if $2+\lambda > 0$ and either $\nu < \nu^-$ or $\nu > \nu^+$, where

$$\nu^{\pm} = -(2+\lambda) \pm 2\sqrt{2+\lambda}. \tag{4.4}$$

Three of the critical points of the (U, V, W) system (Table 1) persist in the (U, W) system: $(0, 0)$, $(\nu, 0)$ and $(\nu$, any $W > 0$ when $\lambda + 2 = 0)$.

In gasdynamics (the (U, V) system) it was possible to find a physically interesting solution for which $U \equiv 1$ throughout. In the (U, W) sub-system, (4.1) and (4.2), U' vanishes on the line $U = 1$ if $\lambda + 2 = 0$. For (4.2) to be consistent in this instance we must have $\nu = 1$ and thus $W(X) = A/X^2$, where A is a constant of integration. To complete the solution $H(X)$ and $G(X)$ must be unravelled from $W(X)$. Equations (2.10) and (2.11) are trivially satisfied in this case. The same issue arose in the consideration of the gasdynamic solution, (3.6)–(3.8), and leads to the need to consider (2.8). Given that $U = 1$, $C = 0$, $\lambda + 2 = 0$ and $\nu = 1$, (2.8) reduces to $H' + H = 0$. Thus, a complete solution is

$$U(X) = 1, \quad G(X) = A, \quad H(X) = \frac{B}{X}, \tag{4.5}$$

with $\nu = 1$ and $\lambda + 2 = 0$. Here B is another constant of integration. Physically

$$u(r,t) = \frac{r}{t}, \quad \rho(r,t) = \frac{A}{r^2}, \quad h(r,t) = \frac{1}{|t|}\frac{B}{X} = \frac{B}{r}. \tag{4.6}$$

However, this solution is dynamically trivial. The magnetic field is purely potential indicating that the magnetic force terms $((r^2h^2)_r/(2r^2)$ in (2.3)) vanish. Consequently this flow is purely kinematic.

Given the trivial nature of the uniform $U \equiv 1$ solution we now consider the possibility that $U = 1$ only at the end-points. For this to be possible a turning point, with $U' = 0$, must exist in the (U, W^+) half-plane. From (4.1) this happens when

$$W = \frac{U(U-1)(U-\nu)}{2+\lambda}. \tag{4.7}$$

This indicates that there is a continuum of such points parameterized by the value of U at the turning point itself. We are constrained to have $W > 0$ and this limits the values at which valid turning points exist; the details depend on the values of λ and ν (see [11]). Numerical experiments show that it is possible to find solutions which join the points $(1, 0)$ and $(1, \infty)$. These end-points are approached at finite values of ξ which we refer to as ξ_∞ and ξ_0, respectively. A local analysis of the system close to the end-points $(1, 0)$ and $(1, \infty)$ shows that $U = 1$ is approached linearly at both end-points, $W(\xi)$ grows algebraically as $(1, \infty)$ is approached and $W = 0$ is approached linearly at $(1, 0)$, the details are summarized in Table 2. In principle,

https://doi.org/10.1017/S0022377808007101 Published online by Cambridge University Press

Table 2. Local behaviour of $U(\xi)$ and $W(\xi)$ near $(1,\infty)$ and $(1,0)$ in the (U,W)-plane.

$(1,\infty)$	$(1,0)$
$U' \sim -(2+\lambda)$ $W \sim \lvert\xi - \xi_\infty\rvert^w \quad w = -(\lambda+2\nu)/(\lambda+2) < 0$	$U' \sim (\nu-1)$ $W' \sim -(\nu-1)^2/(\lambda+\nu+1)$

Table 3. Necessary conditions for (U,W)-subsystems to permit solutions joining $(1,0)$ and $(1,\infty)$.

(i)	$(\xi_\infty > \xi_0)$	$\lambda < -2$	$2\nu+\lambda < 0$	$\nu < 1$	$\lambda+\nu+1 < 0$
(iii)	$(\xi_\infty < \xi_0)$	$\lambda > -2$	$2\nu+\lambda > 0$	$\nu > 1$	$\lambda+\nu+1 > 0$

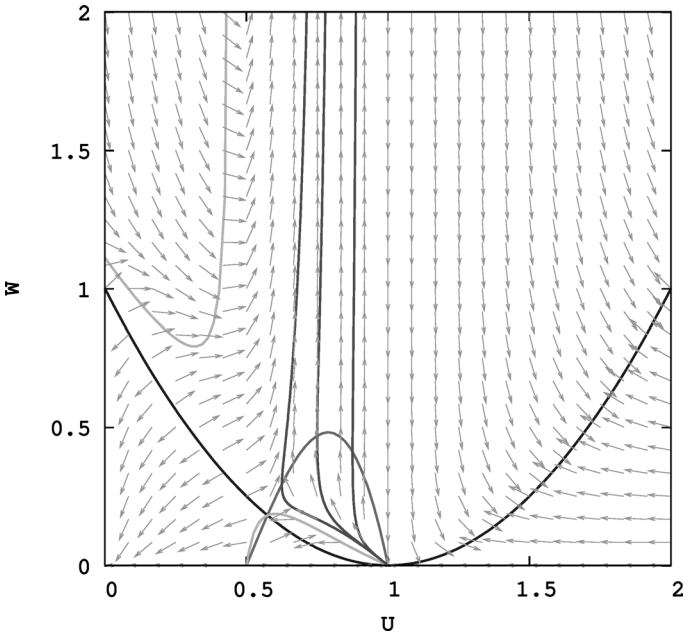


Figure 2. Phase portrait for the (U,W) system with $\nu = 1/2$ and $\lambda = -21/10$. Vectors of (U',W') are scaled to a fixed length. Also shown are three trajectories joining $(1,0)$ and $(1,\infty)$, the null-clines and the singular curve $W = (U-1)^2$.

a solution can join $(1,0)$ and $(1,\infty)$ in one of four different ways: (i) $\xi_\infty > \xi_0$ and $U \leqslant 1$; (ii) $\xi_\infty > \xi_0$ and $U \geqslant 1$; (iii) $\xi_\infty < \xi_0$ and $U \leqslant 1$; and (iv) $\xi_\infty < \xi_0$ and $U \geqslant 1$. By means of the results given in Table 2 it can be established that only cases (i) and (iii) are possible and then only when λ and ν satisfy the constraints given in Table 3.

Figures 2 and 3 show phase portraits for two pairs of values of λ and ν. The sense of direction of the solution changes between the two cases; for $\lambda = -21/10$ and $\nu = 1/2$ the solution joins $(1,0)$ to $(1,\infty)$ whereas for $\lambda = -3/2$ and $\nu = 6/5$ the solution runs from $(1,\infty)$ to $(1,0)$. These are examples of the cases (i) and (iii) discussed above.

https://doi.org/10.1017/S0022377808007101 Published online by Cambridge University Press

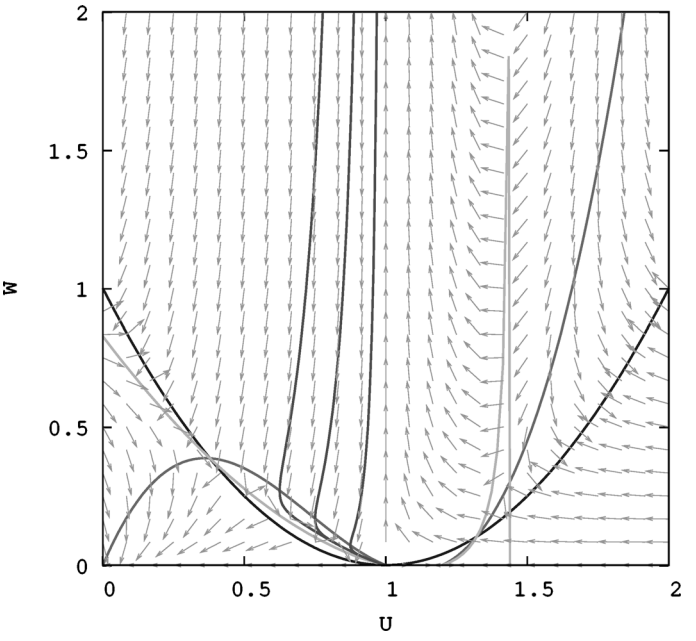


Figure 3. Phase portrait for the (U, W) system with $\nu = 6/5$ and $\lambda = -3/2$. The tangent vectors are scaled to a fixed length. Also shown are the null-clines, the singular curve and three trajectories.

Having established the possibility of constructing annular solutions, we now consider their physical properties. Given W we need to unravel H and G. These can be readily found numerically, given the initial value of either G or H since once one is known the other follows from the definition of W. We perform a local analysis near $(1, 0)$ and $(1, \infty)$ to establish the behaviour of H and G as the end-points are approached [11]. Near $(1, \infty)$, to leading order G behaves like

$$G(\xi) \sim |\xi - \xi_\infty|^{g_\infty}, \quad \text{where } g_\infty = \frac{\lambda + 2\nu}{2 + \lambda} \tag{4.8}$$

while H approaches a constant value at $(1, \infty)$. Near $(1, 0)$ to leading order G and H behave as

$$G(\xi) \sim |\xi - \xi_0|^{g_0}, \quad \text{where } g_0 = -\frac{3\nu + \lambda + 1}{\nu - 1} \tag{4.9}$$

and

$$H(\xi) \sim |\xi - \xi_0|^{h_0}, \quad \text{where } h_0 = \frac{\nu + \lambda + 1}{\nu - 1}, \tag{4.10}$$

respectively.

Figures 4–6 show profiles of $u(r, t)$, $\rho(r, t)$ and $h(r, t)$ as a function of radius at various times for a solution with $\nu = 6/5$ and $\lambda = -3/2$. These are related to the phase portrait shown in Fig. 3. We do not present the equivalent profiles for Fig. 2, $\nu = 1/2$ and $\lambda = -21/10$, because in that instance the flow slows as it collapses since $\nu - 1 < 0$, and this is not the behaviour we expect of an accelerating pinch implosion. From (4.9) and (4.10), in this case both the density and magnetic field are singular at the outer boundary. The magnetic field is constant at the inner

https://doi.org/10.1017/S0022377808007101 Published online by Cambridge University Press

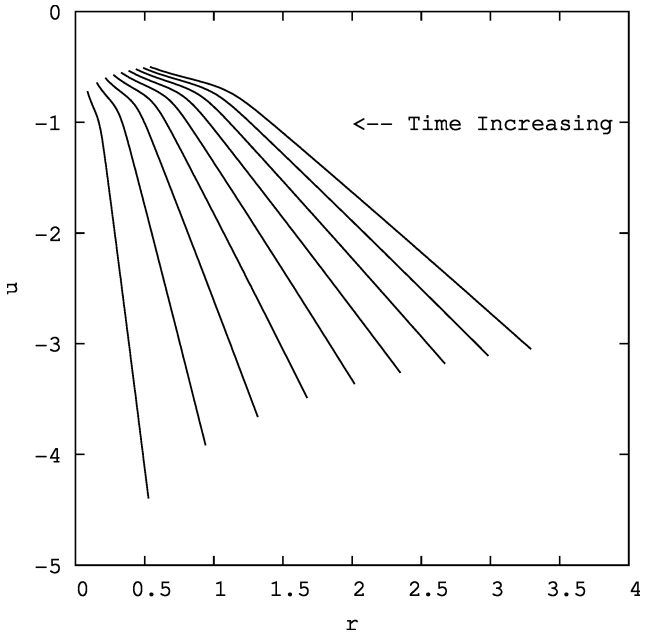


Figure 4. Profiles at equal time intervals of the velocity $u(r,t)$ for a self-similar solution of the (U,W) system with $\lambda = -3/2$ and $\nu = 6/5$.

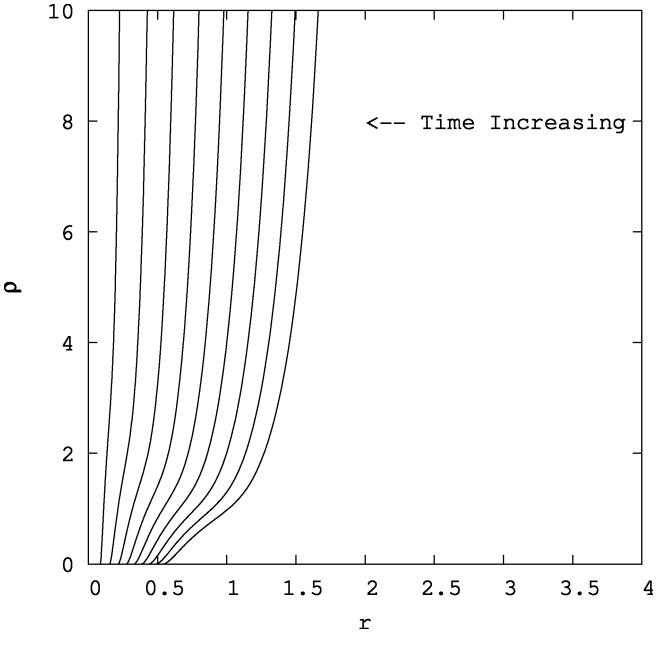


Figure 5. Profiles at equal time intervals of the density $\rho(r,t)$ for a self-similar solution of the (U,W) system with $\lambda = -3/2$ and $\nu = 6/5$.

https://doi.org/10.1017/S0022377808007101 Published online by Cambridge University Press

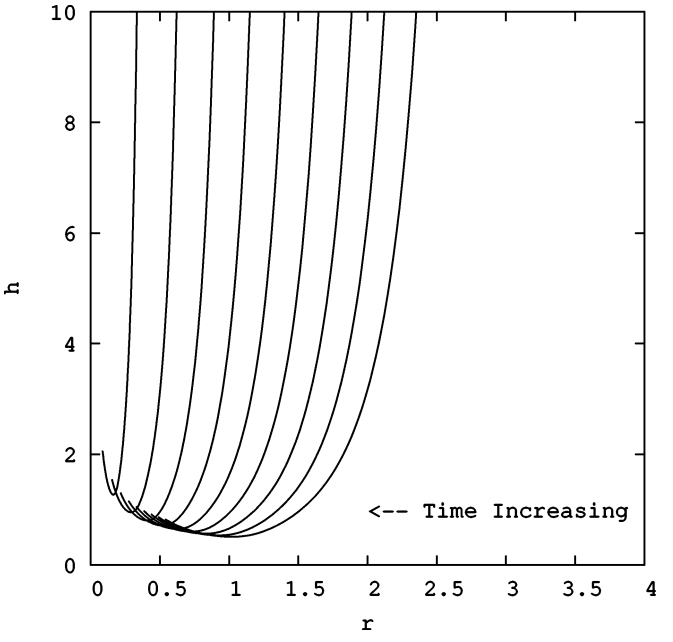


Figure 6. Profiles at equal time intervals of the azimuthal magnetic field $h(r,t)$ for a self-similar solution of the (U,W) system with $\lambda = -3/2$ and $\nu = 6/5$.

boundary, indicating that a source of magnetic field is present inside the annulus. One can imagine that a current carrying wire is present at the axis of symmetry generating a field internal to the flow. This field is amplified by the implosion of the perfectly conducting annulus compressing this internal field; this is reminiscent of the staged z-pinch concept described by Rahman et al. [12]. Alternatively, we may argue that a field which is infinite on the outer boundary and finite at the inner boundary may, on rescaling, plausibly resemble one which is finite on the outer boundary and zero on the inner one.

5. Finite annular solutions of the full (U, V, W) system

Once again, solutions to these equations representing an imploding cylindrical annulus require $U = 1$ at least twice. In the (U,W) system the possibility of a solution for which $U = 1$ for all ξ was ruled out on the grounds that for the required values of the similarity parameters, $\lambda = -2$ and $\nu = 1$, the resulting solution (4.6) is purely kinematic and considered trivial. In an analogous fashion a solution of the full (U,V,W) system with $U \equiv 1$ can be ruled out by the following argument. We desire that both W' and V' be finite on $U = 1$, so that (2.16) requires $\nu = 1$ once again, consequently (2.15) means we must have $\gamma = \nu = 1$. Given $\nu = 1$ and $\gamma = 1$, $U' = 0$ on $U = 1$ implies $(2V(\xi) + W(\xi))(2 + \lambda) = 0$, we rule out $2V(\xi) + W(\xi) = 0$ because it will generally mean that either $W(\xi)$ or $V(\xi)$ will be negative, which is unphysical, and so we conclude that we require $\lambda = -2$. Given $\nu = 1$ and $\gamma = 1$ then (2.15) and (2.16) become

$$V' = -2V, \quad W' = -2W \tag{5.1}$$

https://doi.org/10.1017/S0022377808007101 Published online by Cambridge University Press

and so

$$U(X) = 1, \quad V(X) = \frac{A}{X^2}, \quad W(X) = \frac{B}{X^2}, \tag{5.2}$$

where A and B are constants of integration. A solution with $U \equiv 1$ and $\nu = 1$ will be kinematic, since $u_t + uu_r = 0$ in this case, and so this solution is somewhat trivial. Nevertheless, for the sake of completeness, we calculate the functions $G(X)$ and $H(X)$. Assuming H' and G' are finite with $U \equiv 1$, $\lambda = -2$ and $\nu = 1$ the ODEs governing H' and G' are trivially satisfied and so we turn, again, to (2.8). Since $V(X)$ is no longer identically zero this is slightly more complicated:

$$V' + V\frac{G'}{G} + \frac{(WG)'}{2G} + W = 0. \tag{5.3}$$

Remembering that a prime refers to differentiation with respect to $\ln X$ here, using the definition of W (2.12) to find H given G, we find

$$G(X) = CX^{4A/(2A+B)}, \quad H(X) = \sqrt{BC}X^{-B/(2A+B)}. \tag{5.4}$$

Here C is another constant of integration; we note that if $A = 0$ we recover the equivalent solution of the (U, W) system. It can be shown, as should be expected, that this solution implies $p_r + (r^2h^2)_r/(2r^2) = 0$ for all t and X, and so, again, there is no net force on the fluid. We consider this solution trivial and emphasize the fact that it also requires that $\gamma = 1$, which physically corresponds to an isothermal gas, in order to work.

So the possibility of a solution for which $U \equiv 1$ for all ξ is once again ruled out and the more general requirement of a solution which attains $U = 1$ for two finite values of ξ is considered. Numerical experiments with the (U, V, W) system indicate that solutions of this type do indeed exist, but only for $U \leqslant 1$. These solutions can be thought of as three-dimensional analogues of the solutions discussed in the previous section, because they join the points $(1, 0, 0)$ and $(1, \infty, \infty)$. Figure 7 shows example solutions joining $(1, 0, 0)$ and $(1, \infty, \infty)$ for $\lambda = -3/2$ and $\nu = 2$. Each of the solutions shown corresponds to choosing a different starting point on the $U' = 0$ surface (see (5.5) below), $\xi = 0$ ($X = 1$) at this starting point.

We note that like solutions of the (U, W) system this solution has $U \leqslant 1$ throughout. In the case of the (U, W) system it can be shown that a solution joining $(1, 0)$ and $(1, \infty)$ must have $U \leqslant 1$. Under certain assumptions the analogous result can be established for the full (U, V, W) system. Consider a solution joining $(1, 0, 0)$ and $(1, \infty, \infty)$. Such a solution must have a turning point $(U_0, V_0 > 0, W_0 > 0)$ with $U' = 0$ and so at the turning point

$$2V_0(\gamma U_0 + 1 + \lambda) - \gamma U_0(U_0 - 1)(U_0 - \nu) + \gamma W_0(2 + \lambda) = 0. \tag{5.5}$$

In addition, we expect the turning point to satisfy the constraint

$$(U_0 - 1)^2 - V_0 - W_0 < 0 \tag{5.6}$$

so that it lies above the singular surface. In so doing we neglect the unlikely possibility of a solution joining $(1, 0, 0)$ and $(1, \infty, \infty)$ by crossing the singular surface, at a special point. No such solutions were found in the numerics. Given this constraint a consideration of U'' at the extremal point implies

$$2V_0(\gamma U_0 - \nu)(\gamma U_0 + 1 + \lambda) + \gamma(2 + \lambda)W_0(U_0 - \nu) < 0 \tag{5.7}$$

https://doi.org/10.1017/S0022377808007101 Published online by Cambridge University Press

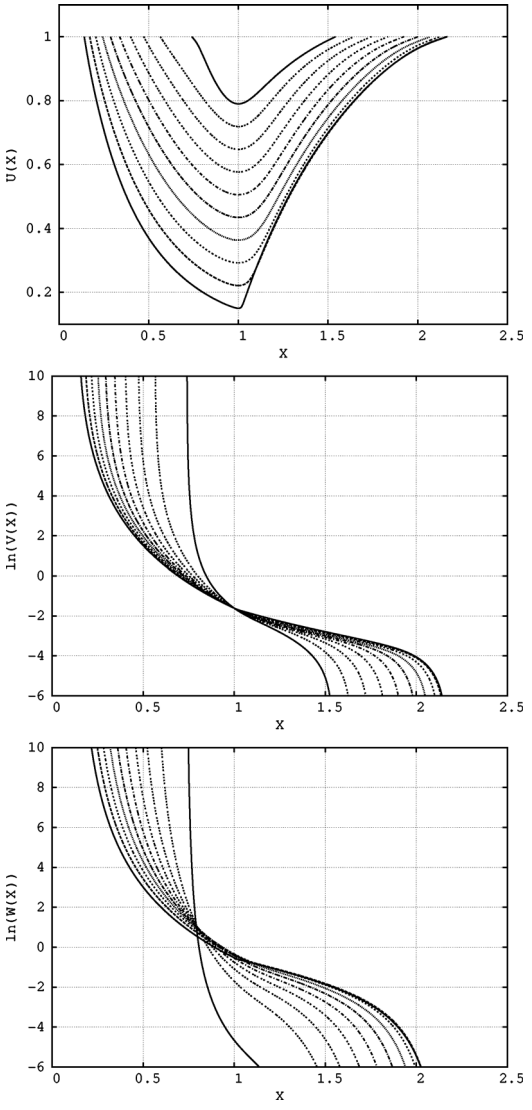


Figure 7. Solutions of the (U, V, W) system with $\lambda = -3/2$ and $\nu = 2$ which join the points $(1, 0, 0)$ and $(1, \infty, \infty)$ and, thus, represent an annulus. Each depicted solution corresponds to choosing a different point of intersection with the surface $U' = 0$. The top plot shows $U(X)$, the middle $\ln V(X)$ and the bottom $\ln W(X)$.

must be satisfied if $U_0 < 1$ and is minimum or $U_0 > 1$ and is maximum. We also assume that

$$\operatorname{sgn}(V'(U_0, V_0, W_0)) = \operatorname{sgn}(W'(U_0, V_0, W_0)). \tag{5.8}$$

This condition is imposed because it is expected that the desirable solution will be a trajectory which joins $(1, 0, 0)$ to $(1, \infty, \infty)$ in a monotonic fashion with respect to $V(\xi)$ and $W(\xi)$; this may be somewhat restrictive but numerical experiments suggest that it is necessary and it further limits the overwhelming choice of possible solutions. Recourse to (2.15) and (2.16) shows, since $U' = 0$ at the point of interest,

https://doi.org/10.1017/S0022377808007101 Published online by Cambridge University Press

that (5.8) is equivalent to either

$$U_0 > \frac{\nu}{\gamma} \quad \text{and} \quad U_0 > \nu \quad \text{or} \quad U_0 < \frac{\nu}{\gamma} \quad \text{and} \quad U_0 < \nu. \tag{5.9}$$

Solutions which join $(1,0,0)$ and $(1,\infty,\infty)$ with $U(\xi) < 1$ for all $\xi \in (\xi_0, \xi_\infty)$ have already been demonstrated numerically. Using these inequalities we consider the possibility of solutions with $U(\xi) > 1$ for all $\xi \in (\xi_0, \xi_\infty)$. For a maximum in $U(\xi)$ it can be shown that the following conditions are necessary:

$$\lambda < -(\gamma U_0 + 1) < -2 \quad \text{and} \quad \frac{\nu}{\gamma} < U_0 < \nu. \tag{5.10}$$

The second of these indicates that $\mathrm{sgn}(V'(U_0, V_0, W_0)) = -\mathrm{sgn}(W'(U_0, V_0, W_0))$, contrary to the assumption (5.8) (and (5.9)). This shows that no λ and ν can be found so that all five constraints, (5.5)–(5.8), can be satisfied at a maximal turning point with $U > 1$.

This strongly suggests that solutions joining $(1,\infty,\infty)$ to $(1,0,0)$ for some $U(\xi) \geqslant 1$ for all ξ are not possible, and no such solutions were found numerically. As demonstrated in Fig. 8, solutions with a maximal turning point with $U > 1$ are possible if the similarity parameters are chosen to satisfy (5.10) (in this example we take $\lambda = -3.02$ and $\nu = 1.3$), but they do not join $(1,0,0)$ and $(1,\infty,\infty)$. The inner boundary, reached when integrating in the $\xi < 0$ direction is the point $(1,\infty,0)$ and the solutions intersect the singular surface $(U-1)^2 - V - W = 0$ at some finite value of ξ when integrated in the $\xi > 0$ direction.

It is, however, possible to have gasdynamic ($W = 0$) annular solutions with $U \geqslant 1$ if $W = 0$. This is suggested by one of the solutions in Fig. 8 which approaches $U = 1$ a second time while W is small but which eventually veers away as W grows.

5.1. The behaviour of solutions local to $(1,\infty,\infty)$

Consider the system local to the point $(1,\infty,\infty)$. Assuming that

$$U(\xi) = 1 + \chi_\infty |\xi - \xi_\infty|^{u_\infty}(1 + A(\xi - \xi_\infty) + \cdots), \quad u_\infty > 0, \tag{5.11}$$

$$V(\xi) = |\xi - \xi_\infty|^{v_\infty}(B + C(\xi - \xi_\infty) + \cdots), \quad v_\infty < 0, \tag{5.12}$$

$$W(\xi) = |\xi - \xi_\infty|^{w_\infty}(D + E(\xi - \xi_\infty) + \cdots), \quad w_\infty < 0, \tag{5.13}$$

near this point the U' equation (2.14) simplifies to

$$U' \sim -\frac{V(2\gamma + 2 + 2\lambda) + \gamma W(2 + \lambda)}{\gamma(V + W)}; \tag{5.14}$$

this suggests three possible scalings, depending on the behaviour of W/V as $\xi \to \xi_\infty$. These are summarized in Table 4; also indicated is the size v_∞ and u_∞ must have relative to each other in each case.

5.2. The behaviour of solutions local to $(1,0,0)$

Local to the $(1,0,0)$ end-point we again assume series expansions of the form

$$U(\xi) = 1 + \chi_0 |\xi - \xi_0|^{u_0} + \cdots, \quad u_0 > 0, \tag{5.15}$$

$$V(\xi) = |\xi - \xi_0|^{v_0}(B + \cdots), \quad v_0 > 0, \tag{5.16}$$

$$W(\xi) = |\xi - \xi_0|^{w_0}(C + \cdots), \quad w_0 > 0; \tag{5.17}$$

https://doi.org/10.1017/S0022377808007101 Published online by Cambridge University Press

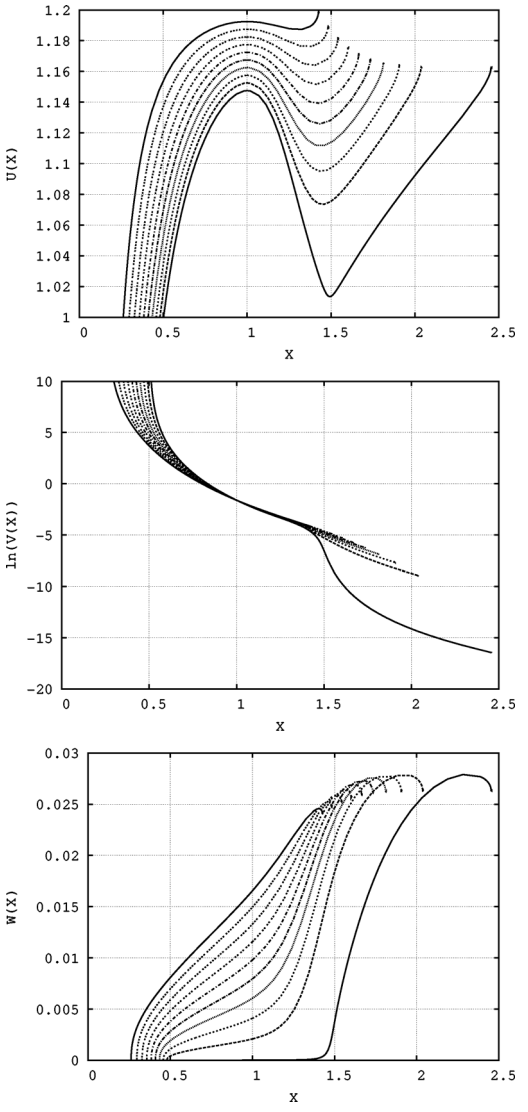


Figure 8. Solutions of the (U, V, W) system with $\lambda = -3.02$ and $\nu = 1.3$. Each depicted solution corresponds to choosing a different point of intersection with the surface $U' = 0$. The top plot shows $U(X)$, the middle $\ln V(X)$ and the bottom $W(X)$. With $U \geqslant 1$, only the solution for which $W \simeq 0$ approaches $U = 1$ a second time.

substituting these into (2.14) for U' gives

$$\chi_0 u_0 |\xi - \xi_0|^{u_0 - 1} = \frac{B|\xi - \xi_0|^{v_0}(2\gamma + 2 + 2\lambda) - \gamma(1-\nu)\chi_0|\xi - \xi_0|^{u_0} + \gamma(2+\lambda)C|\xi - \xi_0|^{w_0}}{\gamma(\chi_0{}^2|\xi - \xi_0|^{2u_0} - B|\xi - \xi_0|^{v_0} - C|\xi - \xi_0|^{w_0})} \tag{5.18}$$

to leading order. This equation suggests various possible scalings for the dependent variables.

https://doi.org/10.1017/S0022377808007101 Published online by Cambridge University Press

Table 4. Summary of the three possible behaviours close to the end-point $(1, \infty, \infty)$ for annular solutions to the (U, V, W) system.

Case	χ_∞	$v_\infty < 0$	$w_\infty < 0$
1. $W/V \to 0$ $(v_\infty < w_\infty < 0)$	$-\dfrac{2\gamma + 2 + 2\lambda}{\gamma}$	$\dfrac{\lambda + 1 - \gamma(\lambda + \nu)}{\lambda + \gamma + 1}$	$-\dfrac{\gamma\nu + \lambda + 1}{\lambda + \gamma + 1}$
2. $V/W \to 0$ $(0 > v_\infty > w_\infty)$	$-(2 + \lambda)$	$\dfrac{2(1-\nu) - \lambda(\gamma - 1)}{2 + \lambda}$	$-\dfrac{2\nu + \lambda}{\lambda + 2}$
3. $V/W \to$ constant $(v_\infty = w_\infty < 0)$	$\dfrac{2(\gamma - 1)}{2 - \gamma}$	$-\dfrac{1 + \nu(\gamma - 2)}{\gamma - 1}$	$= v_\infty$

Firstly, consider the possibility that $2u_0 \leqslant v_0$ and $2u_0 \leqslant w_0$. Then (5.18) indicates

$$\chi_0 u_0 |\xi - \xi_0|^{u_0 - 1} = -\frac{(1-\nu)\chi_0}{{\chi_0}^2 - B - C} |\xi - \xi_0|^{u_0 - 2u_0} \tag{5.19}$$

(note that one of the constants B or C would vanish if $2u_0 < v_0$ or $2v_0 < w_0$, respectively) which requires $u_0 = 1/2$, $v_0 \geqslant 1$ and $w_0 \geqslant 1$. In order to ensure the consistency of this possibility the other ODEs must be considered. The V' and W' equations become

$$\chi_0 |\xi - \xi_0|^{\frac{1}{2}} v_0 B |\xi - \xi_0|^{v_0 - 1} = -B|\xi - \xi_0|^{v_0} \left[\frac{(\gamma - 1)\chi_0}{2|\xi - \xi_0|^{\frac{1}{2}}} + O(1) \right] \tag{5.20}$$

and

$$\chi_0 |\xi - \xi_0|^{\frac{1}{2}} w_0 C |\xi - \xi_0|^{w_0 - 1} = -C|\xi - \xi_0|^{w_0} \left[\frac{\chi_0}{2|\xi - \xi_0|^{\frac{1}{2}}} + O(1) \right], \tag{5.21}$$

respectively; these require

$$v_0 = -\frac{\gamma - 1}{2}, \quad w_0 = -\frac{1}{2}, \tag{5.22}$$

which clearly contradicts the requirements for finite behaviour as $\xi \to \xi_0$ (note that $\gamma > 1$); thus, we rule out the possibility that $u_0 = 1/2$ as $(1, 0, 0)$ is approached.

Considering (5.18) again, in the light of the above discussion, indicates that other possible scalings all require $u_0 = 1$, i.e. U' is $O(1)$. The six possibilities are summarized in Table 5.

Clearly, the behaviour of the system as these end-points are approached must be consistent in that U' must have opposite sign at each end and that $v_0 > 0$, $w_0 > 0$, $v_\infty < 0$ and $w_\infty < 0$ must be satisfied simultaneously. These conditions constrain the values of λ and ν. Studying the 18 possible cases found by combining the results of Tables 4 and 5 reveals that eight have the potential to be possible; it is only a potential because we are only studying one of the necessary conditions required for a solution to join $(1, 0, 0)$ to $(1, \infty, \infty)$; see [11] for further details.

5.3. An example of a MGD solution corresponding to an imploding cylindrical annulus

Figure 9 shows the development of a particular annular self-similar solution as a function of time for $t < 0$ and increasing. In this solution the similarity parameters take the values $\lambda = -3/2$ and $\nu = 2$; so this solution corresponds to one of the solution sets (U, V, W) depicted in Fig. 7.

https://doi.org/10.1017/S0022377808007101 Published online by Cambridge University Press

Table 5. Summary of the six possible types of behaviour for solutions approaching the point $(1,0,0)$ in the (U,V,W) system.

Case	χ_0	$v_0 > 0$	$w_0 > 0$
1	$-\dfrac{2(\gamma-\nu)}{\gamma}$	1	$-\dfrac{\nu(\gamma-1)}{\gamma-\nu} > 1$
2	$-\dfrac{2(\gamma+1+\lambda)}{\gamma}$	$\dfrac{1+\lambda-\gamma(\lambda+\nu)}{\gamma+1+\lambda} < 1$	$-\dfrac{\gamma\nu+1+\lambda}{\gamma+1+\lambda} > v_0$
3	$(\nu-1)$	$-\dfrac{(\gamma-1)(\nu-1)+2(\gamma-\nu)}{\nu-1} > 1$	1
4	$-(2+\lambda)$	$\dfrac{2(\gamma-\nu)-(2+\lambda)(\gamma-1)}{2+\lambda} > w_0$	$\dfrac{2(1-\nu)-(2+\lambda)}{2+\lambda} < 1$
5	$\dfrac{2(\gamma-1)}{2-\gamma}\left(\nu=\dfrac{\gamma}{2-\gamma}\right)$	1	1
6	$\dfrac{2(\gamma-1)}{2-\gamma}$	$-\dfrac{(\gamma-1)+(2-\gamma)(1-\nu)}{\gamma-1} < 1$	$w_0 = v_0$

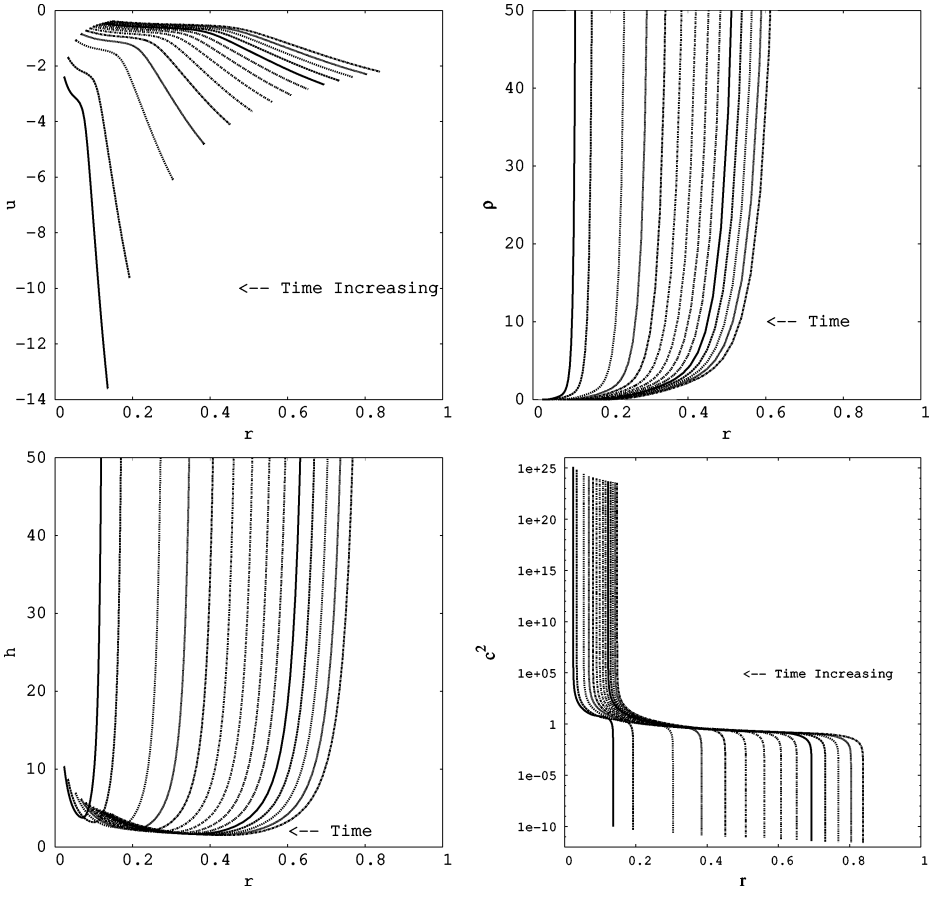


Figure 9. Snapshot profiles of the velocity (top left), density (top right), azimuthal magnetic field (bottom left) and sound-speed squared (bottom right) for a self-similar solution with $\lambda = -3/2$ and $\nu = 2$.

https://doi.org/10.1017/S0022377808007101 Published online by Cambridge University Press

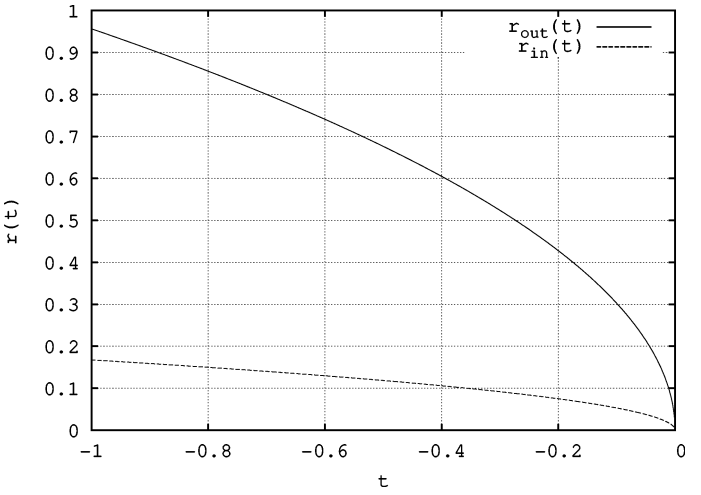


Figure 10. Self-similar inner and outer boundary radii $r_{\rm in}(t)$ and $r_{\rm out}(t)$ for the solution in Fig. 9.

The inner and outer radii $r_{\rm in}(t)$ and $r_{\rm out}(t)$ are drawn in Fig. 10 for this case, which represents the implosion of a z-pinch with a singular collapse at $t = 0$. The inner and outer boundaries of this solution correspond to the points $(1, \infty, \infty)$ and $(1, 0, 0)$, respectively, in the (U, V, W) phase space.

The current flowing through the pinch can be calculated using Ampère's law. The total current inside radius r at time t is

$$I(r,t) = \int_{r_{\rm in}(t)}^{r} J_z(r',t) 2\pi r'\, dr' = \int_{r_{\rm in}(t)}^{r} \frac{1}{r'} \frac{d(r'h(r',t))}{dr'} 2\pi r'\, dr' \tag{5.23}$$

and so

$$I = 2\pi [X^{\lambda+\nu+2} H(X) - X_{\rm in}^{\lambda+\nu+2} H(X_{\rm in})](-t)^{(\lambda+2)/\nu}. \tag{5.24}$$

Thus in the example depicted in Fig. 9, $I \sim (-t)^{\frac{1}{4}}$. This shows that the current in the pinch decreases algebraically as t increases from below towards the time of collapse $t = 0$.

In this example the inner boundary corresponds to the point $(1, \infty, \infty)$ and $U' = \chi_\infty = -(2 + \lambda)$ there, which is case 2 in Table 4. At the outer boundary, corresponding to the point $(1, 0, 0)$, $U' = \chi_0 = -2(\gamma - \nu)/\gamma$, which is case 1 in Table 5. Given the values of U' at the boundaries the behaviour of the flow variables close to the boundary, to leading order, can be determined. A similar analysis was carried out for the (U, W) sub-system in Sec. 4 in some detail, so we simply quote the results here. At the inner boundary as $X \to X_\infty +$, writing $L_\infty := \ln(X/X_\infty)$, we have

$$\begin{aligned} h(X,t) &\sim (-t)^{(\lambda+1)/\nu} \sim (-t)^{-\frac{1}{4}}, \\ \rho(X,t) &\sim {L_\infty}^{(\lambda+2\nu)/(2+\lambda)} (-t)^{2(\lambda+\nu)/\nu} \sim {L_\infty}^{5} (-t)^{\frac{1}{2}}, \\ c(X,t)^2 &\sim {L_\infty}^{(2(1-\nu)-\lambda(\gamma-1))/(2+\lambda)} (-t)^{2/\nu-2} \sim {L_\infty}^{-2} \frac{1}{(-t)} \end{aligned} \tag{5.25}$$

https://doi.org/10.1017/S0022377808007101 Published online by Cambridge University Press

and at the outer boundary $X \to X_0-$, writing $L_0 := \ln(X_0/X)$, leads to

$$\begin{aligned} h(X,t) &\sim {L_0}^{(2\nu+\gamma\lambda)/2(\gamma-\nu)}(-t)^{(\lambda+1)/\nu} \sim {L_0}^{-\frac{9}{4}}(-t)^{-\frac{1}{4}}, \\ \rho(X,t) &\sim X{L_0}^{(\nu(\gamma+1)+\lambda\gamma)/2(\gamma-\nu)}(-t)^{2(\lambda+\nu)/\nu}, \\ &\sim {L_0}^{-\frac{17}{2}}(-t)^{\frac{1}{2}}, \\ c(X,t)^2 &\sim L_0\frac{1}{(-t)}. \end{aligned} \tag{5.26}$$

These results show that at the inner boundary the density vanishes, the magnetic field is constant and the sound-speed is singular, whilst at the outer boundary the density and magnetic field are singular, and the sound-speed vanishes. The behaviour of the fluid pressure, $p \sim \rho c^2$, can be inferred from these results. As the inner boundary is approached

$$p(X,t) \sim {L_\infty}^3(-t)^{-\frac{1}{2}} \tag{5.27}$$

is regular, except at the singularity at $t = 0$, and at the outer boundary

$$p(X,t) \sim {L_0}^{-\frac{15}{2}}(-t)^{-\frac{1}{2}} \tag{5.28}$$

is singular. It is interesting that in this solution the fluid pressure at the inner boundary vanishes but the magnetic field and magnetic pressure are finite and non-zero. This requires that some (relatively small) current is present in the cavity. From (5.24), we see that since $H(X) \sim \ln[X/X_0]^{-9/4}$ as $X \to X_0-$, the total current flowing through the cylinder is infinite. The current inside $[X_{\rm in}, X < X_{\rm out}]$ is finite but decreasing with time.

6. On the attractiveness of annular solutions

In this section we explore whether the self-similar solutions described in Sec. 5 are attractive. By this we mean that, given some fairly arbitrary initial conditions and appropriate boundary conditions, do solutions of the full ideal MGD initial value problem approach the self-similar solutions?

Related numerical work was performed by Glasser [13] who examined the time evolution of solid fibre z-pinches, including finite resistivity, finite viscosity and radiation losses. Glasser briefly considers the ideal MGD similarity solutions of Liberman and Velikovich [5], although he considers that the ideal assumption is not appropriate to the physical problem of the fibre pinch. He found that initiating numerical calculations (with the non-ideal terms switched off) with suitable initial conditions led to good agreement between the numerics and the self-similar solutions. Whereas Glasser's work is concerned with solid, cylindrical pinches we are concerned with ideal MGD annular *implosions*.

We solve the initial value problem in the Lagrangian form

$$\rho\frac{Du}{Dt} = -p_r - \frac{(r^2h^2)_r}{2r^2}, \tag{6.1}$$

$$\frac{D\rho}{Dt} = -\rho\frac{(ru)_r}{r}, \tag{6.2}$$

https://doi.org/10.1017/S0022377808007101 Published online by Cambridge University Press

$$\rho \frac{De}{Dt} = -p \frac{(ru)_r}{r}, \tag{6.3}$$

$$\frac{Dh}{Dt} = -hu_r, \tag{6.4}$$

$$\frac{Dr}{Dt} = u. \tag{6.5}$$

In this form we require the equation of state

$$p = (\gamma - 1)e\rho. \tag{6.6}$$

Here we work with the energy equation (6.3) rather than the sound-speed evolution equation, but this system is equivalent to (2.1)–(2.4) and sound-speed is readily deduced.

Details of the numerical algorithm can be found in [11]. The consistency of this scheme was established by showing that solutions which evolve from initial conditions taken from a sub-domain of the similarity solution described in Sec. 5 (the solution with $\lambda = -3/2$ and $\nu = 2$ depicted in Fig. 9) remain self-similar; details can again be found in [11].

We can impose boundary conditions on (6.1)–(6.6) in various ways, each having different physical connotations. We can impose known time profiles of the boundary velocity, the external boundary pressure or electrical current; this last part implies a magnetic pressure when combined with the boundary radius. We consider each of these possibilities. The details of the imposed boundary conditions depend on the similarity parameters; we specify $\lambda = -3/2$ and $\nu = 2$ throughout the remainder of this section.

We must also provide appropriate initial conditions. To do this we first choose an initial time $t_0 < 0$ and two values, X_{in} and X_{out}, of the similarity variable corresponding to the inner and outer radial boundaries of the flow. Given these choices and the similarity parameter ν we can define the initial spatial domain by $\mathscr{D} := \{r \mid X_{\text{in}}|t_0|^{1/\nu} \leqslant r \leqslant X_{\text{out}}|t_0|^{1/\nu}\}$. Initial data must be provided for the velocity u, density ρ, specific energy e and magnetic field h for all $r \in \mathscr{D}$. We take these initial functions to be constant for ρ, e and h and u is a linear function of radius interpolated between the values u_{in} and u_{out}. The boundary conditions also follow from the choice of X_{in}, X_{out} and t_0.

If we impose velocity boundary conditions on the annular surfaces these will, by definition, move self-similarly. However, as demonstrated by Fig. 11 globally the solution is not attracted to a similarity solution. In Fig. 11 we have plotted $U(r,t) := \nu(t/r)u(r,t)$ against $X(r,t) = r/(-t)^{1/\nu}$. If the solution approached a similarity solution these curves would be attracted to a single curve as the collapse evolves. We also note that the flow develops a shock discontinuity, these can be included in the similarity solution [5,11] but will move self-similarly therein. Figure 12 plots the radial position of the inner and outer boundaries and of the shock, showing that unlike the surfaces, the shock does not move self-similarly in this solution. Indeed, it is reflected from the inner boundary and later from the outer boundary.

Figure 13 shows a radius versus time plot of surfaces from a calculation in which the boundary magnetic field is imposed; the field is an algebraic function of time,

https://doi.org/10.1017/S0022377808007101 Published online by Cambridge University Press

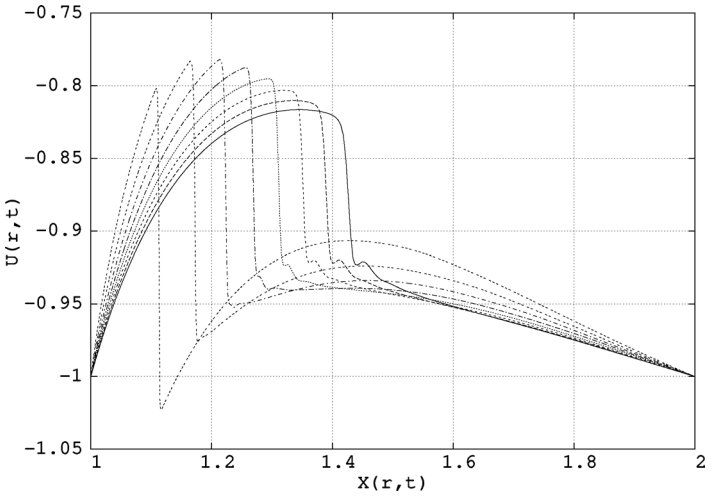


Figure 11. Transformed velocity profile snapshots for a MGD initial value calculation for $\tau = 99$ to $\tau = 99.7$ with $\Delta\tau = 0.1$. Collapse occurs at $\tau = 100$.

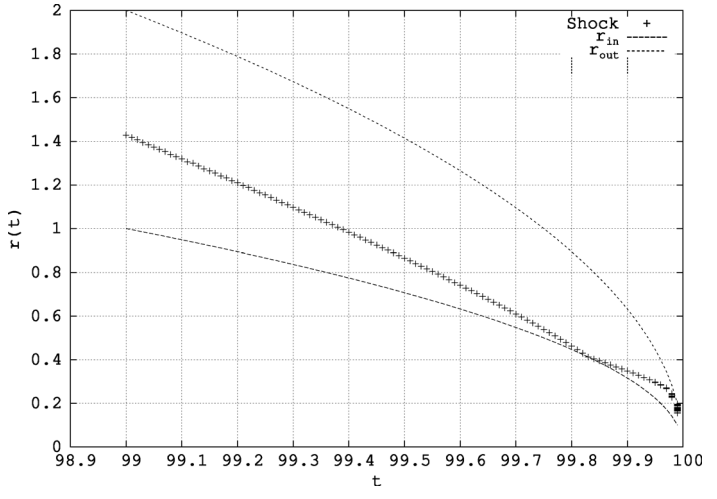


Figure 12. Evolution of the inner and outer boundaries for a MGD initial value calculation. The middle curve shows the position of a shock wave as a function of time, which is seen to reflect from the boundaries of the annulus.

$h_b \sim |t|^{(\lambda+1)/\nu}$. In this case the surfaces of the annulus no longer exhibit self-similar motion.

Finally, in Fig. 14 we show the behaviour of the inner and outer radii of the annulus which result from an imposed total current. The imposed current (see (5.24)) is of the form $I(t) \sim |t|^{(\lambda+\nu)/2}$ corresponding to a surface magnetic field $h_{\rm b}(t) \sim I(t)/r_{\rm b}(t)$, where $r_{\rm b}(t)$ is the boundary radius predicted by the solution of the initial value problem. Again in this case the behaviour of the annular surfaces is far from self-similar.

https://doi.org/10.1017/S0022377808007101 Published online by Cambridge University Press

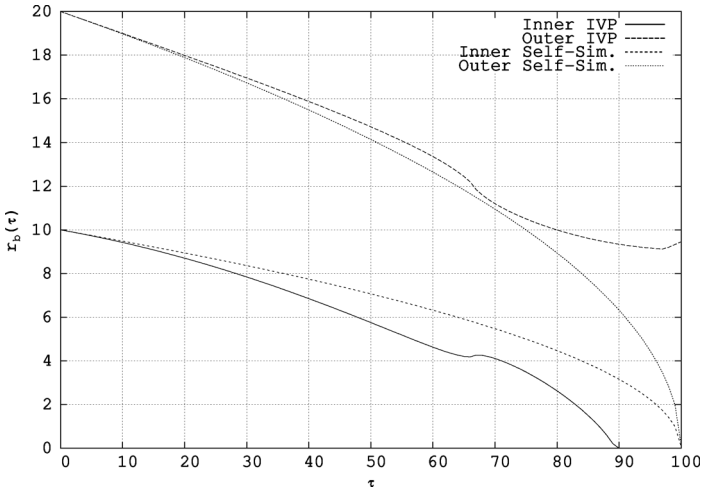


Figure 13. Numerically calculated inner and outer radii for the case $\nu = 2$ and $\lambda = -3/2$. Also shown are the corresponding radii for a self-similar solution.

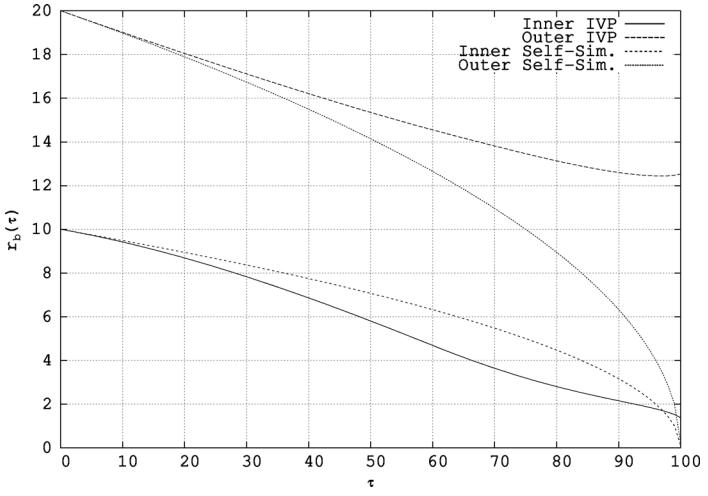


Figure 14. The numerically calculated time behaviour of the inner and outer boundaries for the magnetogasdynamic equations with fixed current boundary conditions using $\nu = 2$ and $\lambda = -3/2$. Also shown are the corresponding self-similar inner and outer radii.

7. Concluding remarks

We have considered and demonstrated cylindrical finite annular self-similar solutions to the equations of gasdynamics, ideal $\beta = 0$ plasma motion and ideal MGD with the aim of modelling imploding liner z-pinches.

The gasdynamic solution studied is the cylindrical equivalent of Kidder's spherical solution [10]. The ideal $\beta = 0$ solutions exhibit singular behaviour at their outer boundary in both the magnetic field and density. The ideal MGD solutions have singular behaviour in some subset of the flow variables at both the inner and outer boundaries. Numerically we are unable to find ideal MGD similarity solutions which

https://doi.org/10.1017/S0022377808007101 Published online by Cambridge University Press

describe the implosion of hollow annuli while crossing the limiting characteristic (singular) at a special point. Theoretical arguments suggest that such behaviour is highly unlikely but we have not proved this rigorously. Although not described here, it is possible to construct ideal MGD similarity solutions with shock discontinuities by matching solutions of the form described here to an internal jump boundary condition obtained from the Hugoniot relations [5, 11]. Doing this adds little that is essentially new to the details of the similarity solutions.

We considered the ideal MGD initial value problem numerically in an attempt to study whether these self-similar solutions are attractive by taking suitably general initial conditions and various types of appropriate boundary condition. Numerical calculations stubbornly refuse to exhibit attraction to a self-similar asymptotic state.

It is possible that these numerical solutions are not attracted to a self-similar solution because of the choice of initial conditions. A particularly simple, structure-free, set of initial conditions was chosen, on the grounds that we are trying to determine whether self-similar solutions are attractive starting from arbitrary initial conditions if the appropriate boundary conditions are applied. Naturally, some choices of initial conditions are expected to lead to self-similar behaviour in some region.

We have shown that a self-similar solution does not evolve from a general initial profile. This is the case not only near the end-points, where the similarity solutions become singular, but also in the fluid interior. The ideal MGD equations are somewhat restrictive, in particular because of magnetic flux freezing. The magnetic field does not develop naturally from a null state, as it would in practice, but is determined by the initial condition and subsequent flow. It thus retains a memory of the initial imposed field.

This reflection leads us to consider extending the equations to include effects of finite resistivity. With the inclusion of diffusive terms an initial magnetic field evolves more naturally, and it will be shown in a subsequent paper that similarity solutions are still possible.

References

[1] Ryutov, D. D., Derzon, M. S. and Matzen, M. K. 2000 The physics of fast z-pinches. *Rev. Mod. Phys.* **72**.

[2] Hammer, J. H. et al. 1996 Two-dimensional radiation-magnetohydrodynamic simulations of SATURN imploding z-pinches. *Phys. Plasmas* **3**(5), 2063–2069.

[3] Marder, B. M., Sanford, T. W. L. and Allshouse, G. O. 1998 Numerical simulations of annular wire-array z-pinches in (x, y), (r, θ) and (r, z) geometries. *Phys. Plasmas* **5**(8), 2997–3005.

[4] Peterson, D. L. et al. 1998 Characterisation of energy flow and instability development in two-dimensional simulations of hollow z pinches. *Phys. Plasmas* **5**(9), 3302–3310.

[5] Liberman, M. A. and Velikovich, A. L. 1986 Self-similar motions in z-pinch dynamics. *Nucl. Fusion* **26**, 709–728.

[6] Van Guderley, G. 1942 Starke kugelige und zylindrische verdichtungsstöße in der nähe des kugelmittelpunktes bzw. der zylinderachse. *Luftfahrtforschung* **19**, 302–312.

[7] Meyer-ter-Vehn, J. and Schalk, C. 1982 Selfsimilar spherical compression waves in gas dynamics. *Z. Naturforsch* **37a**, 955–969.

[8] Jeffrey, A. 1966 *Magnetohydrodynamics*. Oliver and Boyd.

[9] Acheson, D. J. 1990 *Elementary Fluid Dynamics*. Oxford: Oxford University Press.

https://doi.org/10.1017/S0022377808007101 Published online by Cambridge University Press

[10] Kidder, R. E. 1976 Laser-driven compression of hollow shells: power requirements and stability limitations. *Nucl. Fusion* **16**, 3–14.

[11] Lock, R. M. 2007 Aspects of the magnetohydrodynamic z-pinch. Imperial College, University of London.

[12] Rahman, H. U., Ney, P., Wessel, F. J. and Rostoker, N. 1997 Staged pinch for controlled thermonuclear fusion. *J. Plasma Phys.* **58**, 367–379.

[13] Glasser, A. H. 1989 A moving finite element model of the high density z-pinch. *J. Comput. Phys.* **85**(1), 159–209.

https://doi.org/10.1017/S0022377808007101 Published online by Cambridge University Press